Effect of the Pauli principle on photoelectron spin transport in p + GaAs

Fabian Cadiz, D. Paget, A. Rowe, Thierry Amand, Philippe Barate, S. Arscott

Effect of the Pauli principle on photoelectron spin transport in p^+ GaAs

F. Cadiz,[1] D. Paget,[1] A. C. H. Rowe,[1] T. Amand,[2] P. Barate,[2] and S. Arscott[3]
[1]*Physique de la Matière Condensée, Ecole Polytechnique, CNRS, 91128 Palaiseau, France*
[2]*Université de Toulouse, INSA-CNRS-UPS, 31077 Toulouse Cedex, France*
[3]*Institut d'Electronique, de Microélectronique, et de Nanotechnologie (IEMN), Université de Lille, CNRS, Avenue Poincaré, Cité Scientifique, 59652 Villeneuve d'Ascq, France*
(Received 25 February 2015; revised manuscript received 7 April 2015; published 17 April 2015)

In p^+ GaAs thin films, the effect of photoelectron degeneracy on spin transport is investigated theoretically and experimentally by imaging the spin polarization profile as a function of distance from a tightly focused light excitation spot. Under degeneracy of the electron gas (high concentration, low temperature), a dip at the center of the polarization profile appears with a polarization maximum at a distance of about 2 μm from the center. This counterintuitive result reveals that photoelectron diffusion depends on spin, as a direct consequence of the Pauli principle. This causes a concentration dependence of the spin stiffness while the spin dependence of the mobility is found to be weak in doped material. The various effects which can modify spin transport in a degenerate electron gas under local laser excitation are considered. A comparison of the data with a numerical solution of the coupled diffusion equations reveals that ambipolar coupling with holes increases the steady-state photoelectron density at the excitation spot and therefore the amplitude of the degeneracy-induced polarization dip. Thermoelectric currents are predicted to depend on spin under degeneracy (spin Soret currents), but these currents are negligible except at very high excitation power where they play a relatively small role. Coulomb spin drag and band-gap renormalization are negligible due to electrostatic screening by the hole gas.

DOI: 10.1103/PhysRevB.91.165203 PACS number(s): 72.25.Ba, 72.25.Dc

I. INTRODUCTION

Recently, a number of novel phenomena occurring during spin-dependent transport in semiconductors have been reported, including the spin Hall effect [1], the inverse spin Hall effect [2], the spin Coulomb drag effect [3], and the spin helix [4]. These phenomena are of interest in and of themselves and also because they may affect the operation of a large number of proposed semiconductor spintronic devices [1,5–7]. Experimental investigations including the use of novel techniques such as spin gratings [8] or spin noise [9] reveal that these phenomena arise from one of two possible coupling mechanisms, either spin-charge or spin-spin couplings. In the former, the spin-orbit interaction plays a central role and gives rise to the extrinsic spin Hall effect and the spin helix, as well as providing the basis for the electrical manipulation of spin [10–12]. Spin-spin coupling, on the other hand, results in spin Coulomb drag [3] and a spin-dependent density of states via band-gap renormalization [13]. Recently a new spin-charge coupling phenomenon resulting from Pauli blockade in a degenerate electron gas was revealed [14], resulting in a spin dependence of the diffusion constant as large as 50%. Pauli blockade had been implicitly included in some theoretical treatments of spin-polarized electron transport [13,15,16], but had not yet been explicitly detailed or experimentally demonstrated. It is of importance since it will naturally modify all other coupling phenomena in the degenerate limit.

Here, we present a theoretical and experimental investigation of the effect of degeneracy on spin transport in p^+ GaAs using a polarized microluminescence method in which the spin polarization is measured as a function of distance from a local, diffraction-limited excitation spot [17–19]. This study reveals that the dominant effect of degeneracy is the spin dependence of diffusion. Ambipolar coupling to the photocreated hole distribution is of central importance for the observation of the effects since it acts to locally increase the electron density near the excitation spot and therefore to increase the degree of degeneracy. A detailed theoretical analysis allows us to predict two other spin-dependent transport effects induced by degeneracy. These effects are (i) spin-dependent thermoelectric currents (spin-Soret effect) [20] caused by the radial temperature gradients, and (ii) spin dependence of the mobility, which is strongly decreased by hole screening of the electron collisions with charged impurities in the p^+ material considered here. These two effects are shown, using an extensive sample characterization, to be negligible here and their demonstration requires specific experimental configurations and doping levels. Coulomb spin drag and spin-dependent band-gap renormalization effects are also negligible because of electrostatic screening by the majority holes. Finally, it is shown that the usual spin-grating technique [8] is not adapted to the observation of Pauli blockade coupling phenomena since only spin concentration gradients are created whereas both spin and charge concentration gradients are necessary.

The structure of the paper is as follows. The experimental section (Sec. II) contains a description of the method, a presentation of the results, and a semiquantitative interpretation. The theory presented in Sec. III considers spin transport in a semiconductor under local light excitation, for which the charge and spin densities, as well as the temperature, vary as a function of space. Section IV describes the relative efficiencies of the various possible mechanisms for spin transport, while the quantitative interpretation of the results is presented in Sec. V.

II. EXPERIMENTAL

A. Method

For the experimental investigation of charge and spin diffusion, we have used p^+ GaAs films of thickness $d = 3$ μm,

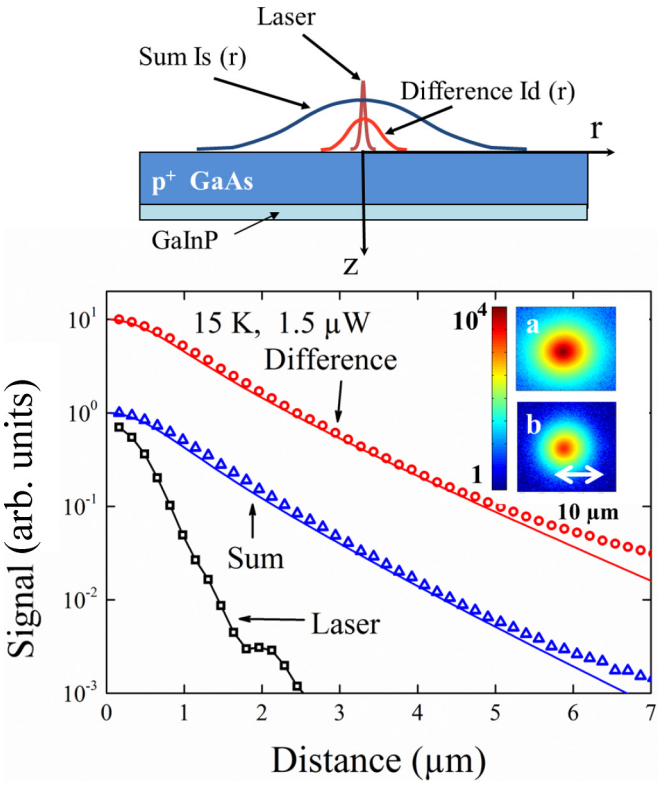

FIG. 1. (Color online) Top panel: Principle of the experiment on p^+ GaAs passivated at the bottom surface by a thin GaInP layer, with a naturally oxidized front surface. The circularly polarized laser is tightly focused (Gaussian radius 0.45 μm) on the GaAs film and the spatial distribution of the luminescence sum signal [Eq. (1), image a] and difference signal [Eq. (2), image b] is imaged using a modified commercial microscope. The ratio of the two profiles, not shown here, gives the spin polarization profile [Eq. (3)]. The figure shows angular-integrated cross sections of the laser beam profile and of the above images, shifted vertically for clarity, fitted with numerical solutions of the diffusion equations [Eq. (4) and Eq. (5)], which yield estimates of the effective diffusion lengths $L_e^{\rm eff}$ and $L_s^{\rm eff}$.

grown on a GaAs semi-insulating substrate with, as shown in the top panel of Fig. 1, a thin GaInP back layer to confine the photoelectrons and to ensure a negligible recombination velocity $S' = 0$ at the bottom GaAs surface. The top surface is naturally oxidized.

The principle of the experimental technique is shown in Fig. 1 and has been presented in more detail elsewhere [17]. Circularly polarized light excitation at 1.59 eV is focused to a Gaussian spot of half width $\omega = 0.6$ μm. The photoluminescence (PL) of the sample only comes from the layer since emission of the semi-insulating substrate is negligible. One measures the PL intensity profile for which the cross section as a function of radial distance r from the excitation spot is related to the electronic concentration $n(r,z)$ by

$$I_s(r) = A \int_0^d n(r,z) \exp[-\alpha_l z] dz, \tag{1}$$

where A is a proportionality constant and $\alpha_l \approx (3\ \mu\text{m})^{-1}$ is the absorption coefficient at the luminescence energy [21].

For a circularly polarized excitation, one also measures the profile of the difference between the σ^+- and σ^--polarized components of the luminescence. Its cross section is related to the spin density $s = n_+ - n_-$ where $n_\pm$ are the concentrations of electrons of spin $\pm$, taking the z axis for quantization of the electronic spins, and is given by

$$I_d(r) = -A \int_0^d s(r,z) \exp[-\alpha_l z] dz. \tag{2}$$

Finally, the profile of the electronic spin polarization $\mathscr{P}(r) = s/n$ is given by

$$I_d(r)/I_s(r) = \mathscr{P}(r)\mathscr{P}_i, \tag{3}$$

where $\mathscr{P}_i = (g_+ - g_-)/(g_+ + g_-)$ such that $g_\pm$ is the spatially dependent rate of creation of electrons of spin $\pm$. The quantity $g_\pm$ depends on the matrix elements of the allowed optical transitions and is equal to ± 0.5 for $\sigma^\mp$ light excitation [22].

The densities $n(r,z)$ and $s(r,z)$ are, respectively, solutions of the continuity equations

$$(g_+ + g_-) - n/\tau + \frac{1}{q}\vec{\nabla} \cdot (\vec{J}_c) = 0, \tag{4}$$

$$(g_+ - g_-) - s/\tau_s + \frac{1}{q}\vec{\nabla} \cdot (\vec{J}_s) = 0. \tag{5}$$

Here q is the absolute value of the electronic charge, $1/\tau = K_r(N_A + \delta p)$, and $1/\tau_s = 1/\tau + 1/T_1$, where N_A is the acceptor density, δp is the density of photocreated holes, and K_r is the bimolecular recombination coefficient. Since the spin relaxation time T_1 is long with respect to the various times which characterize spin transport, one considers separately the currents $\vec{J}_+$ and $\vec{J}_-$ of $+$ and $-$ spins so that, in a simple picture at low density, $\vec{J}_c = \vec{J}_+ + \vec{J}_- = qD\vec{\nabla}n$ and $\vec{J}_s = \vec{J}_+ - \vec{J}_- = qD_s\vec{\nabla}s$, where D and D_s are the charge and spin diffusion constants. These equations are solved by imposing (i) electron currents at the front ($z = 0$) and back surface ($z = d$) that are equal to $qSn(0)$ and $-qS'n(d)$, respectively. Here S and S' are the corresponding recombination velocities. (ii) Spin currents equal to $qSs(0)$ and $-qS's(d)$, respectively. One can then define an effective lifetime $\tau_{\rm eff}$ which takes into account bulk and surface recombination and an effective spin lifetime $\tau_{\rm seff}$ such that $1/\tau_{\rm seff} = 1/\tau_{\rm eff} + 1/T_1$ [19]. Charge and spin effective diffusion lengths are defined as $L_e^{\rm eff} = \sqrt{D\tau_{\rm eff}}$ and $L_s^{\rm eff} = \sqrt{D_s\tau_{\rm seff}}$.

Figure 1 also shows the sum and difference images at 15 K at a very low excitation power of 1.5 μW, as well as their angular-integrated cross sections. As seen from the cross section of the laser profile, the sum and difference signals are observed well beyond the laser spot, and reveal charge and spin diffusion of photoelectrons after creation, respectively. Analysis of these profiles, using Eq. (1), Eq. (2), Eq. (4), and Eq. (5), gives $L_e^{\rm eff} = 1.42$ μm and $L_s^{\rm seff} = 1.25$ μm at $T = 15$ K and shows that the spin relaxation time, T_1, is larger than the electron lifetime.

B. Sample characterization

Hall effect measurements on an identical contacted sample [23] have shown that, at $T = 15$ K, as in agreement with independent studies [24], the concentration of ionized

acceptors is $N_A^- \approx 10^{18}\,\mathrm{cm}^{-3}$, close to its value at 300 K. The hole mobility is $200\,\mathrm{cm}^2/\mathrm{V\ s}$. On the same contacted sample, the electron mobility was measured as a function of T_e by monitoring the change of the luminescence profile induced by application of an electric field [25]. One finds $\mu_e = 8800\,\mathrm{cm}^2/\mathrm{V\ s}$ at $T_e = 50$ K and $\mu_e = 5800\,\mathrm{cm}^2/\mathrm{V\ s}$ at $T_e = 75$ K. Using Einstein's relation at low power, this gives $D_0 \approx 37\,\mathrm{cm}^2/\mathrm{s}$.

Time-resolved polarized luminescence measurements as a function of T_e were also performed in the same GaAs sample [26]. At $T_e = 50$ K, one finds $\tau_{\mathrm{eff}} \approx 335$ ps and $T_1 \approx 1125$ ps. While at $r = 0$, T_1 can be smaller than the latter value, its value would still be much larger than the diffusion time [Eq. (7)], so that its possible decrease will very weakly affect the electronic polarization. As a result, $T_1 \approx 1125$ ps was taken in all cases. For this relatively large acceptor doping and low temperature, there is no doubt that the dominant mechanism for electronic spin relaxation is the Bir-Aronov-Pikus one, originating from exchange interaction with holes [27].

C. Experimental investigation of spin transport

1. *Polarization profiles as a function of power*

Panel (a) of Fig. 2 shows the profiles of the electronic polarization $\mathscr{P}$, at $T = 15$ K for increasing excitation powers, as obtained using Eq. (3) (the other panels are calculations to be explained in Sec. IV below). Curve a, taken at the same low power as Fig. 1, reveals the expected polarization decrease caused by spin-lattice relaxation during transport [17]. Note that the low-power electronic polarization at $r = 0$, $\mathscr{P}^{lp}(0) = 45\%$ is almost equal to the initial polarization $\mathscr{P}_i$. Since as will be shown below the spin relaxation time of thermalized electrons is much larger than their lifetime at the excitation spot, the slight difference is attributed to spin-lattice relaxation during thermalization. As a result, in Eq. (4) and Eq. (5), g_+ and g_- must be replaced by g_+^* and g_-^*, respectively, such that $g_+^*(0)/g_-^*(0) = [1 + \mathscr{P}^{lp}(0)]/[1 - \mathscr{P}^{lp}(0)]$.

As the power is increased, a polarization dip at $r = 0$ progressively appears. At 2.5 mW, the polarization at $r = 0$ is 28%, while at $r \approx 2\ \mu$m, it is 42%, slightly larger than its low-power value at the same distance from the excitation spot. If the power is further increased, the profiles, not shown here, exhibit an overall decrease of the polarization because of heating of the electron gas by the laser.

In agreement with the dependencies of the polarization dip as a function of excitation power and temperature, it has been shown [14] that this effect occurs because of Pauli blockade in the degenerate photoelectron gas, i.e., when either one or both of n_+ and n_- become larger than the spin-resolved effective density of states in the conduction band N_c^s, given by

$$N_c^s = (1/2)N_c^0(T_e/300)^{3/2}, \tag{6}$$

where $N_c^0 = 4.7 \times 10^{17}\,\mathrm{cm}^{-3}$ and T_e is the temperature of the electron gas. In this case, the diffusion constant is larger for majority spin electrons (D_+) than for minority spin electrons (D_-). The more efficient removal by diffusion away from $r = 0$ induces a depletion of majority electrons at $r = 0$, with a relative accumulation at some distance away from $r = 0$. This effect is illustrated in the inset of Fig. 2(a) which shows the spatial dependencies of n_+ and n_-. In this framework, the ratio of D_+/D_- can be estimated by considering a simple two-dimensional picture, where the concentrations $n_\pm$ are replaced by their averages $\langle n_\pm \rangle$ over z, and by writing that the diffusion time out of the excitation spot is, within numerical factors of order unity, given by

$$\tau_{\mathrm{eff}}^0(\langle n_\pm \rangle) \approx \omega^2/4D_\pm, \tag{7}$$

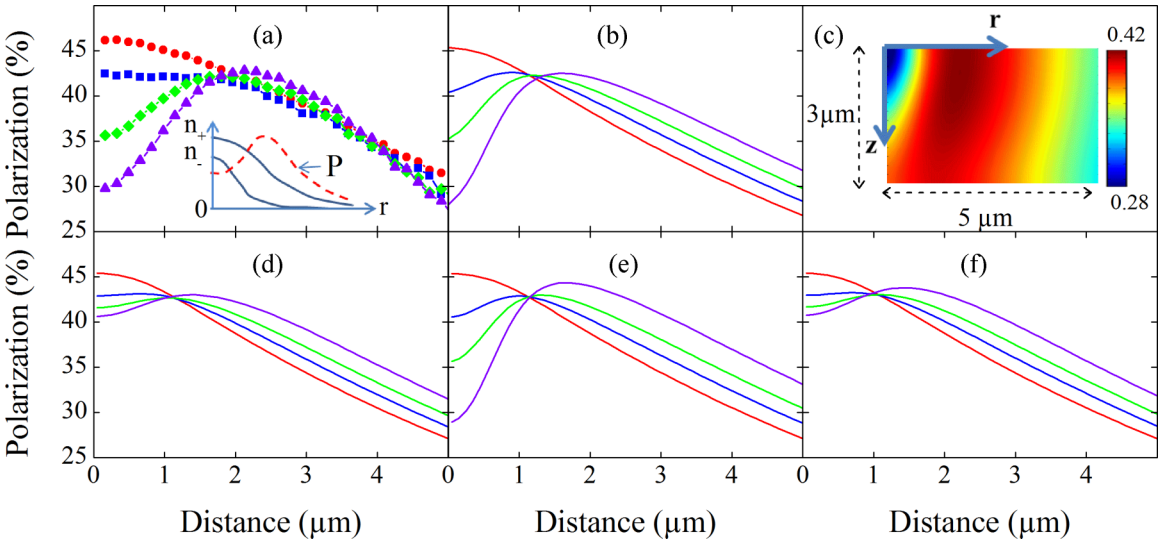

FIG. 2. (Color online) Panel (a) shows the experimental polarization profiles at $T = 15$ K as a function of excitation power: 28 μW (filled circles), 1 mW (filled squares), 1.9 mW (filled diamonds), 2.5 mW (filled triangles). The inset of panel (a) interprets the formation of a polarization dip, as caused by the larger diffusion length of majority electrons, which induces a depletion of these electrons at $r = 0$. Panel (b) shows the corresponding calculated profiles including all effects which modify spin transport. Panel (c) shows the image of the calculated spatial distribution of the polarization for an excitation power of 2.5 mW. With respect to panel (b), the profiles of panel (d) do not consider ambipolar diffusion, those of panel (e) do not consider thermoelectric currents, and those of panel (f) neglect both ambipolar diffusion and temperature gradients and thus illustrate the conditions of spin-grating experiments.

and is of the order of several ps, that is, shorter than characteristic times for recombination and spin relaxation. Considering that diffusion is the dominant process for removal of electrons from the excitation spot, the spin concentrations at $r = 0$ are given by

$$\langle n_{\pm}\rangle \approx g^{*}_{\pm}(0)\tau^{0}_{\mathrm{eff}}(\langle n_{\pm}\rangle). \tag{8}$$

One then obtains the following very simple result, in which the poorly known numerical factors of Eq. (8) are eliminated:

$$D_{+}/D_{-} = \frac{1+\mathscr{P}^{lp}(0)}{1-\mathscr{P}^{lp}(0)} \times \frac{1-\mathscr{P}(0)}{1+\mathscr{P}(0)}. \tag{9}$$

At high power, we find $D_{+}/D_{-} \approx 1.49$ implying that degeneracy causes a significant spin dependence of the diffusion constant. Writing to first order

$$D_{\pm} = D^{*}[1 \pm \delta\mathscr{P}], \tag{10}$$

where the expressions for D^{*} and δ will be given below, one finds $\delta = 0.65$.

2. Spin-dependent charge diffusion

The effective charge diffusion constant, defined as $\langle D\rangle = (1/n)\sum_i n_i D_i$, is found using Eq. (10) and given by

$$\langle D\rangle = D^{*}[1+\delta\mathscr{P}^{2}], \tag{11}$$

which implies that the sum profile under degeneracy depends on spin via a second-order effect. In order to show such effect, the sum profiles I_{σ} for a circularly polarized (σ) excitation were compared with the profiles I_{π} for a linearly polarized excitation (π, so that $\mathscr{P} = 0$), keeping the excitation power constant to within 0.1%. Figure 3 shows the relative difference of these profiles at $T = 15$ K for different power densities. At low power (curve d), the signal is zero within experimental uncertainty, showing that charge transport in nondegenerate conditions does not depend on spin. In contrast, when the excitation power is increased, there progressively appears a depletion of photoelectrons at $r = 0$. This depletion, of the order of 2.5%, is compensated by a converse excess of photoelectrons at a distance larger than about 1.5 μm. This shows that the diffusion constant of spin-polarized electrons is larger than for spin-unpolarized electrons created by π excitation.

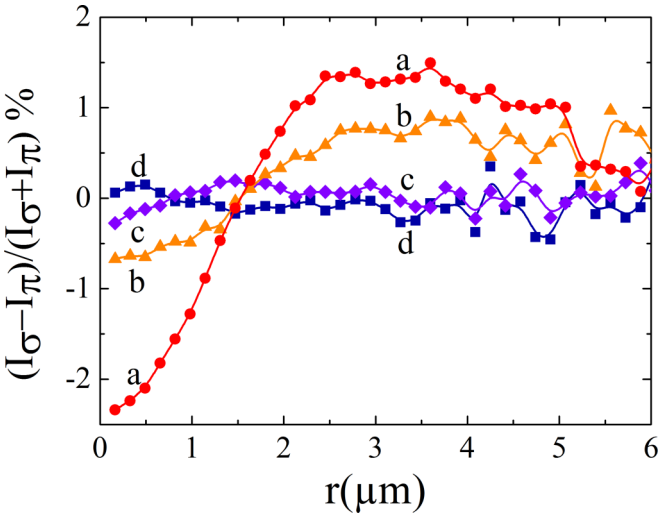

FIG. 3. (Color online) Relative difference between the luminescence intensity profiles obtained under circularly polarized excitation (σ) and under linearly polarized excitation (π), for different excitation powers, (a) 2.3 mW, (b) 0.9 mW, (c) 0.4 mW, and (d) 65 nW. For each excitation power, the only difference is the polarization of the photoelectron gas. A difference of the order of 2.5% between both intensity profiles is observed at high power at $r = 0$, revealing the spin-dependent diffusion of photoelectrons.

Using Eq. (11), the spin dependence of the charge concentration at $r = 0$ is given by

$$\frac{\langle n_{\sigma}\rangle - \langle n_{\pi}\rangle}{\langle n_{\sigma}\rangle + \langle n_{\pi}\rangle} = \frac{\langle D_{\pi}\rangle - \langle D_{\sigma}\rangle}{\langle D_{\pi}\rangle + \langle D_{\sigma}\rangle} = -\frac{\delta\mathscr{P}^{2}}{2+\delta\mathscr{P}^{2}}, \tag{12}$$

from which we obtain, in agreement with the preceding subsection, $\delta = 0.58$.

3. Polarization profiles as a function of excitation light polarization

In order to investigate the dependence of the effect of Pauli blockade on electronic polarization, the helicity of the excitation light is changed in order to change $\mathscr{P}_i$. Panel (a) of Fig. 4 shows the corresponding polarization profiles at 2.5 mW. These profiles show that the dip at $r = 0$ indeed decreases with decreasing $\mathscr{P}_i$ without, as shown in panel (b), any significant modification of the overall polarization profile. As shown in panel (c), the electronic polarization at $r = 0$ is proportional to $\mathscr{P}_i$. This behavior is in agreement with the predictions made using Eq. (9) and Eq. (10), according to which, to first order in $\mathscr{P}$, one has $\mathscr{P}(0) = \mathscr{P}^{lp}(0)/(1+\delta)$. From the slope of this behavior, one finds $\delta = 0.45$, in qualitative agreement with the value of the preceding subsection.

4. Kinetic energy effects

The luminescence and polarization spectra can be monitored as a function of r by using a scanned multimode

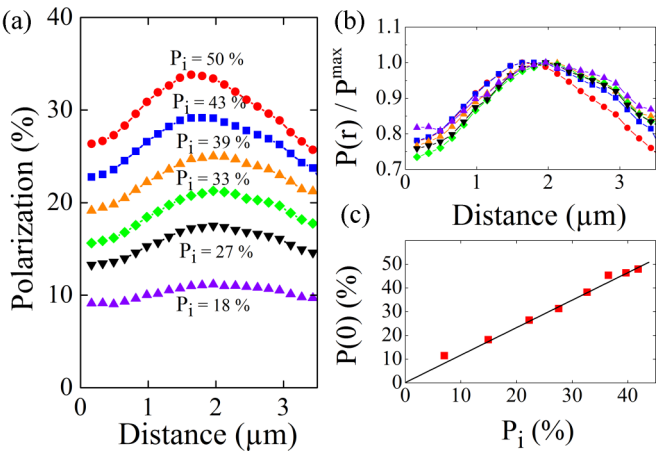

FIG. 4. (Color online) Panel (a) shows the polarization profiles for decreasing values of the initial polarization $|\mathscr{P}_i|$ and panel (b) shows the same curves normalized to the polarization maximum near 2 μm. As shown in panel (c), the electronic polarization at $r = 0$ is proportional to $\mathscr{P}_i$, thus revealing that the ratio D_{+}/D_{-} depends linearly on electronic polarization.

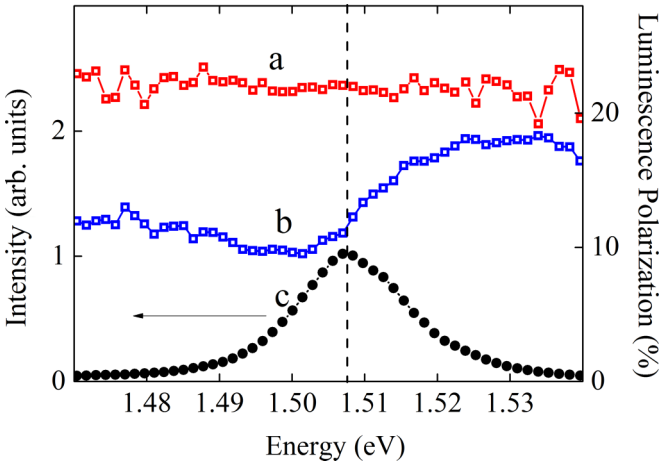

FIG. 5. (Color online) Dependence of spin polarization on kinetic energy. Curve a and curve b show the spatially resolved polarization spectrum at $r = 0$ and at 15 K for a power of 28 μW and 2.5 mW, respectively. Curve c shows for comparison the intensity spectrum at 2.5 mW at the place of excitation. Comparison between curves a and b shows that the Pauli blockade effect is smaller for hot electrons.

optical fiber that captures PL over a spot size of 0.9 μm. The fiber is then coupled to a spectrometer to yield a local spectrum like those shown in Fig. 5. The fact that the luminescence lies at an energy smaller than the GaAs band gap (1.519 eV at this temperature) has been interpreted as due to band-gap renormalization caused by the free hole population (Refs. [28,29]). In nondegenerate conditions (curve a), the polarization does not depend on light energy and is consistent with the electronic polarization at $r = 0$ in panel (a) of Fig. 2. As expected, in degenerate conditions (curve b), the overall polarization is weaker than for curve a because of the spin-dependent transport effects discussed above. However, this polarization decrease is mostly observed on the low-energy side of the spectrum, while for energies above 1.52 eV, the two spectra almost coincide. It is concluded that the spin filter effect decreases with increasing kinetic energy in the conduction band.

As suggested in Ref. [30] in the case of [110] quantum wells, it is tempting to conclude that the depolarization of thermalized electrons at $r = 0$ rather arises from an increased efficiency of the local spin relaxation processes, caused by the larger hole concentration or by the increased temperature. This hypothesis cannot explain the results for three main reasons: (i) Such polarization loss can only concern electrons localized in potential fluctuations, since diffusive electrons will transmit their depolarization after diffusion. However, localized electrons only appear at lattice temperatures smaller than 10 K and are absent at the present higher temperature [26]. (ii) Since the effective lifetime at $r = 0$ is $\omega^2/4D \approx 10$ ps, the polarization decrease would require an extremely strong, unphysical, decrease of T_1 from its value of 1125 ps at low power [26]. (iii) Since an increased spin relaxation at $r = 0$ does not affect the charge, the present hypothesis cannot explain the observed dependencies of the charge diffusion on intensity and polarization reported in Fig. 3.

III. THEORY

A. Charge and spin unipolar diffusion equations

The charge and spin currents $\vec{J}_c$ and $\vec{J}_s$ which appear in the diffusion equations [Eq. (4) and Eq. (5)] are expressed as the sum of contributions of diffusive charge and spin currents, of drift currents due to internal electric fields of ambipolar origin, and of thermoelectric currents caused by local heating of the photoelectron gas: $\vec{J}_{c(s)} = \vec{J}^{dr}_{c(s)} + \vec{J}^{dif}_{c(s)} + \vec{J}^{T}_{c(s)}$, where each of these contributions is the sum and difference of the corresponding spin currents, respectively. These currents are calculated below.

1. Drift currents

The drift current of electrons of spin i is given by $\vec{J}^{dr}_i = \vec{E}\sum_j \sigma_{ij}$, where the nondiagonal elements of the conductivity matrix σ_{ij} reflect the coupling between opposite spins (spin Coulomb drag), mostly originating from electron-electron collisions [3,13,15]. It is given by

$$\sigma_{ij} = q n_i \mu_i \alpha_{ij}, \tag{13}$$

where the mobility μ_i of electrons of spin i is given by

$$\mu_i = q\tau_{mi}/m^*. \tag{14}$$

The momentum relaxation time τ_{mi}, calculated in Appendix A using the Boltzmann equation formalism, is equal to

$$\tau_{mi} = -\frac{2}{3}\frac{\int \tau_m(\varepsilon)\varepsilon^{3/2}(\partial f_{0i}/\partial\varepsilon)d\varepsilon}{\int \varepsilon^{1/2} f_{0i} d\varepsilon}, \tag{15}$$

where f_{0i} is the Fermi distribution and ε is the kinetic energy. Here, $\tau_m(\varepsilon)$ is assumed to be of the form [16,31]

$$\tau_m(\varepsilon) \propto \varepsilon^p, \tag{16}$$

where p depends on the scattering process which determines the mobility. The concentration dependence of μ_i is obtained using Eq. (14) and Eq. (15). One finds

$$\mu_i = \mu_0 \zeta(n_i) = \mu_0 \frac{\mathscr{F}^*_{p+1/2}(\eta_i)}{\mathscr{F}^*_{1/2}(\eta_i)}, \tag{17}$$

where μ_0 is the mobility in nondegenerate conditions, $\eta_i = E_{Fi}/k_B T_e$, where E_{Fi} is the Fermi energy and k_B is the Boltzmann constant, and where the Fermi integral $\mathscr{F}^*_k(\eta_i)$ is given by

$$\mathscr{F}^*_k(\eta_i) = \frac{1}{\Gamma(k+1)}\int_0^\infty \frac{x^k dx}{1+\exp(x-\eta_i)}. \tag{18}$$

Here η_i is related to the electronic spin concentration by

$$n_i = N^s_c \mathscr{F}^*_{1/2}(\eta_i). \tag{19}$$

The coefficients α_{ij}, given by [15]

$$\alpha_{ij} = \frac{\tau_{ee}\delta_{ij} + (n_j/n)\tau_{m,-i}}{\tau_{ee}+\tau_m}, \tag{20}$$

account for the conductivity changes of each spin reservoir caused by the spin-spin couplings. Here δ_{ij} is the Kronecker symbol. The time τ_{ee} is given by $n\tau_{ee} = \tau_{ee,i} n_{-i}$, where τ_{eei} is the collision time for an electron with spin i with an electron

of opposite spin. The spin-averaged time τ_m is given by

$$\tau_m = (n_+/n)\tau_{m-} + (n_-/n)\tau_{m+}. \tag{21}$$

One has finally $\vec{J}_c^{dr} = \sigma_c \vec{E}$ and $\vec{J}_s^{dr} = \sigma_s \vec{E}$, where $\sigma_c = \sum_{ij} \sigma_{ij}$ and $\sigma_s = \sum_{ij} i\sigma_{ij}$.

2. *Diffusive currents*

The diffusive current of electrons of spin i depends on the spatial gradients of the Fermi energies E_{Fj}, and is given by $q\vec{J}_i^{dif} = \sum_j \sigma_{ij}(\vec{\nabla}_r E_{F_j}|_{T_e})$, where the spatial gradient of the Fermi energy at constant temperature of the electron gas T_e is expressed as $\vec{\nabla}_r E_{F_j}|_T = \sum_i S_{ji}\vec{\nabla}_r n_i$, where the spin stiffness matrix is given by

$$S_{ij} = \frac{\partial E_{F_i}}{\partial n_j}. \tag{22}$$

Note that the total Fermi level gradient is given by $\vec{\nabla}_r E_{F_j} = \vec{\nabla}_r E_{F_j}|_{T_e} + (\partial E_{F_j}/\partial k_B T_e)\vec{\nabla}_r k_B T_e$. However, the second term contributes to the thermoelectric current and will be considered in the following subsection. The diffusive current can be rewritten as

$$\vec{J}_i^{dif} = q(D_{ii}\vec{\nabla} n_i + D_{i,-i}\vec{\nabla} n_{-i}), \tag{23}$$

where the elements of the diffusion matrix D are given by

$$qD_{ij} = \alpha_{ii} n_i \mu_i S_{ij} + \alpha_{i,-i} n_{-i}\mu_{-i} S_{-i,j}. \tag{24}$$

Equation (24) is the generalized Einstein relation. The charge and spin diffusive currents are finally given by

$$\frac{1}{q} J_c^{dif} = D_{cc}\vec{\nabla} n + D_{cs}\vec{\nabla} s, \tag{25}$$

$$\frac{1}{q} J_s^{dif} = D_{sc}\vec{\nabla} n + D_{ss}\vec{\nabla} s, \tag{26}$$

where the diffusion constants are linear combinations of the D_{ij} given by $2D_{cc} = \sum_{ij} D_{ij}$ and $2D_{ss} = \sum_{ij} ij D_{ij}$, $2D_{cs} = \sum_{ij} j D_{ij}$ and $2D_{sc} = \sum_{ij} i D_{ij}$, and can be straightforwardly calculated if the spin stiffness matrix S_{ij} is known. It is concluded that two types of spin-related mechanisms can affect charge and spin diffusion. Spin-spin couplings result in a nondiagonal D_{ij} matrix, because of which a gradient of spins j affects the diffusive current of spins i. Charge-spin and spin-charge couplings originate from nonzero values of D_{cs} and D_{sc}, respectively, and result in a dependence on the spin (charge) current on the charge (spin) density.

3. *Thermoelectric currents: Soret charge and spin currents*

The thermoelectric current of electrons of spin i is calculated in Appendix A by solving the Boltzmann equation. It is of the form $\vec{J}_i^T = -\sum_j \sigma_{ij}\mathscr{S}_j \vec{\nabla}_r T_e$ and $\mathscr{S}_j$ is the spin-dependent Seebeck coefficient for which the value for unpolarized electrons is equal to its usual value given elsewhere [32]. It is given by $\mathscr{S}_j = -(1/qT_e)(E_{Tj} - \gamma_j k_B T_e)$, where

$$E_{Ti} = \frac{\int \tau_m(\varepsilon)\varepsilon^{3/2}(\partial f_{0i}/\partial\varepsilon)d\varepsilon}{\int \tau_m(\varepsilon)\varepsilon^{1/2}(\partial f_{0i}/\partial\varepsilon)d\varepsilon}, \tag{27}$$

where γ_i depends on the Fermi integral $\mathscr{F}_k(\eta) = \Gamma(k+1)\mathscr{F}_k^*(\eta)$ and is given by

$$\gamma_i = \frac{\mathscr{F}_{1/2}(\eta_i)}{\mathscr{F}_{-1/2}(\eta_i)}. \tag{28}$$

The above equations are similar to those of the Seebeck effect in which there is however no current [20]. Here the spin currents arise through a distinct effect, which has been described by Soret [33] for mass transport. The current $\vec{J}_i^T$ will be hereafter called the Soret current. Here, it is more convenient to express it in the form

$$\vec{J}_i^T = q\sum_j \vec{K}_{ij} n_j. \tag{29}$$

The Soret velocity matrix $\vec{K}_{ij}$ is given by

$$q\vec{K}_{ij} = \alpha_{ij}\mu_j\left(\frac{E_{Tj}}{k_B T_e} - \gamma_j\right)\vec{\nabla}_r(k_B T_e). \tag{30}$$

The currents $\vec{J}_{cT}$ and $\vec{J}_{sT}$ defined in Eq. (4) and Eq. (5) are finally given by

$$\frac{1}{q}\vec{J}_c^T = \vec{K}_{cc} n + \vec{K}_{cs} s, \tag{31}$$

$$\frac{1}{q}\vec{J}_s^T = \vec{K}_{sc} n + \vec{K}_{ss} s, \tag{32}$$

where $2\vec{K}_{cc} = \sum_{ij}\vec{K}_{ij}$, $2\vec{K}_{ss} = \sum_{ij} ij\vec{K}_{ij}$, $2\vec{K}_{sc} = \sum_{ij} i\vec{K}_{ij}$, and $2\vec{K}_{cs} = \sum_{ij} j\vec{K}_{ij}$.

B. Ambipolar diffusion equations

Taking account of all contributions defined in the preceding section, the diffusion equations for electrons and spins can finally be written

$$(g_+ + g_-) - n/\tau + \vec{\nabla}\cdot\left[(\vec{E}/q)\sigma_c + D_{cc}\vec{\nabla} n + D_{cs}\vec{\nabla} s + \vec{J}_c^T\right] = 0, \tag{33}$$

$$(g_+ - g_-) - s/\tau_s + \vec{\nabla}\cdot\left[(\vec{E}/q)\sigma_s + D_{sc}\vec{\nabla} n + D_{ss}\vec{\nabla} s + \vec{J}_s^T\right] = 0. \tag{34}$$

In order to take account of the electrostatic coupling between electrons and the slower diffusing holes, it is further necessary to couple these equations with the diffusion equation for spin-unpolarized holes, which is

$$(g_+ + g_-) - \delta p/\tau + \vec{\nabla}\cdot[-(\vec{E}/q)\sigma_h + D_h\vec{\nabla}\delta p] = 0, \tag{35}$$

where δp is the photohole concentration and D_h is the hole diffusion constant. Here $\sigma_h = q(N_A^- + \delta p)\mu_h$ is the conductivity, where μ_h is the hole mobility. The thermoelectric hole current is neglected since the local heating of the hole gas is weak [34]. The electric field satisfies Poisson's equation

$$\vec{\nabla}\cdot\vec{E} = \frac{e}{\epsilon\epsilon_0}(\delta p - n), \tag{36}$$

where ϵ is the dielectric constant and ϵ_0 is the permittivity of free space. Equations (33), (34), (35), and (36) are solved numerically, as shown in Appendix B, by imposing that, in addition to the boundary conditions for Eqs. (4), (5) defined

in Sec. II A, the hole currents at the front ($z = 0$) and back surface ($z = d$) are equal to $qS\delta p(0)$ and $-qS'\delta p(d)$.

IV. RELEVANT MECHANISMS FOR SPIN TRANSPORT UNDER LOCAL EXCITATION OF p^+ MATERIAL

A. Effect of degeneracy on diffusion and its spin dependence

As already shown in Ref. [14], degeneracy can induce a spin dependence of the diffusion constant due to two distinct effects which are direct consequences of the Pauli principle. The first one is the concentration dependence of the spin stiffness [Eq. (22)]. Neglecting electron-electron interactions which will be shown below to be screened by the hole gas, the spin stiffness matrix is diagonal and, in Eq. (13), $\alpha_{ij} = \delta_{ij}$. Using Eq. (19), one finds $S_{ii} = k_B T_e/[\mathscr{F}^*_{-1/2}(\eta_i)N_c^s]$ and Eq. (24) reduces to the spin-uncoupled Einstein equation for a degenerate electron gas [35]

$$D_i = \frac{n_i \mu_i}{q} S_{ii} = \xi(n_i)\mu_i \frac{k_B T}{q}, \tag{37}$$

where $\xi = n_i S_{ii}/k_B T_e$ is given by

$$\xi(n_i) = \frac{\mathscr{F}^*_{1/2}(\eta_i)}{\mathscr{F}^*_{-1/2}(\eta_i)} = 2\gamma_i. \tag{38}$$

This quantity is unity for a nondegenerate gas and increases with concentration.

The second possible effect induced by degeneracy is a spin-dependent increase of the mobility, as described by Eq. (17), and is a direct consequence of Pauli exclusion due to which elementary scattering processes are forbidden if the final state is already occupied by an electron of the same spin. The diffusion constants for spins $\pm$ are finally given by

$$D_i = D_0 \nu(n_i), \tag{39}$$

where $D_0 = \mu_0 k_B T_e/q$ and

$$\nu(n_i) = \xi(n_i)\zeta(n_i) = \frac{\mathscr{F}^*_{p+1/2}(\eta_i)}{\mathscr{F}^*_{-1/2}(\eta_i)}. \tag{40}$$

Using the linearized form defined by Eq. (10), the charge and spin diffusion constants which appear in Eq. (33) and Eq. (34) are finally given

$$D_{cc} = D_{ss} = D_0 \nu(n/2), \tag{41}$$

$$D_{cs} = D_{sc} = D_0 \nu(n/2)\delta\mathscr{P}, \tag{42}$$

where the two quantities δ and D^* introduced in Eq. (10) are now given a precise definition. Here $\delta = d\ln[\nu(n/2)]/d\ln(n/2)$ and is equal to $2(p+1)/3$ at large degeneracy, while $D^* = D_0\nu(n/2)$. The Pauli principle induces a coupling between the charge and spin diffusions, for which the coupling coefficients $\delta\mathscr{P}$ are identical in the two equations. They increase with electron polarization and concentration.

For highly p-doped GaAs and $T_e = 50$ K, curve a of Fig. 6 shows the concentration dependence of the Fermi energy E_{F_i}. Degeneracy is achieved for electronic concentrations larger than $10^{16}\,\mathrm{cm}^{-3}$, for which $E_{Fi} > 0$. As shown in the same panel, the reduced diffusion constant increases with concentration from its values of 1 in nondegenerate conditions. For $p = 3/2$, it is found that the spin dependence of the spin

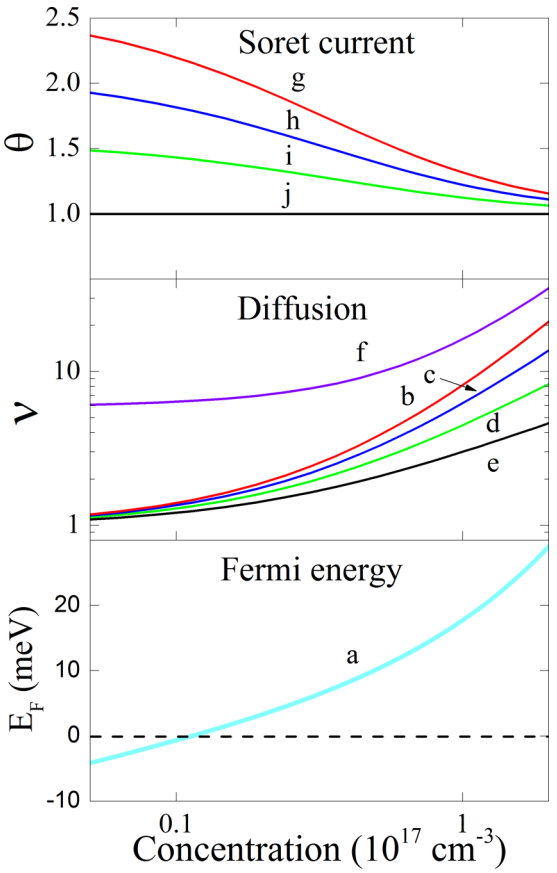

FIG. 6. (Color online) The bottom panel shows, at $T_e = 50$ K, the Fermi energy as a function of the spin-resolved photoelectron concentration n_i (curve a) revealing the onset of degeneracy near $n = 10^{16}\,\mathrm{cm}^{-3}$. The dependence of the reduced diffusion constant ν [Eq. (40)] is shown for selected values of p, as defined by Eq. (16): 3/2 (b), 1 (c), 1/2 (d), 0 (e). Curve f shows this same quantity for $p = 3/2$, but for hot electrons, of kinetic energy larger than $k_B T_e$. The top panel shows the quantity θ [Eq. (44)] on which depends the Soret current, for $p = 3/2$ (g), 1 (h), 1/2 (i), 0 (j).

stiffness and of the mobility have an equal importance in the spin dependence of the diffusion since the increase of ξ and ζ, not shown in the figure, are quite similar. When p is decreased, the concentration dependence of the mobility becomes reduced, which induces as shown in the figure, a reduction of the concentration and spin dependence of the diffusion constant. For a typical electron gas of density $n_+ + n_- = 10^{17}\,\mathrm{cm}^{-3}$ and $p = 3/2$, with a spin polarization of $\mathscr{P} = (n_+ - n_-)/n = 40\%$, one finds $D_+/D_- \approx 2.2$. For $p = 0$, this ratio is reduced to $D_+/D_- \approx 1.3$ for the same values of $n_\pm$. However, because of the smaller diffusion constant with respect to $p = 3/2$, the concentration at $r = 0$ is increased in order to verify Eq. (8), so that the effect of p on the actual spin dependence of D is rather weak.

The above calculations can be extended to hot electrons in order to explain the results of Fig. 5. Using a restriction of the Fermi integrals appearing in Eq. (28) and Eq. (17) to electrons of kinetic energy larger than $\epsilon_{\min}$ reduces the spin stiffness and the concentration dependence of ξ. This is the same for the mobility because the rate of occupation of electronic states at

the corresponding kinetic energy is smaller, so that scattering by an ionized impurity is less likely to be forbidden by the Pauli principle. Curve f of Fig. 6, calculated using $\epsilon_{\min} = k_B T_e$ and in the particular case of $p = 3/2$, shows that the concentration dependence of ν is significantly reduced and explains the weaker spin dependence of the diffusion constant of hot electrons.

B. Spin Soret current under degeneracy

Under the sole effect of the thermal gradient, the Soret velocities are given by $K_{cc} = K_{ss} = [K_{++} + K_{--}]/2$ and $K_{cs} = K_{sc} = [K_{++} - K_{--}]/2$ while $K_{+-} = K_{-+} = 0$. The ratio of the unipolar diffusive $[J_c^{dif}]$ and Soret currents is then given by

$$\frac{J_c^T}{J_c^{dif}} = \theta \frac{\vec{\nabla}_r T_e/T_e}{\vec{\nabla}_r n/n}. \tag{43}$$

The dimensionless quantity θ, given by

$$\theta = \frac{E_T}{\xi k_B T} - 1/2, \tag{44}$$

is related to the Seebeck constant defined in Sec. III A3 by $\mathscr{S} = -(k_B/q)\xi\theta$ and is for spins i given by

$$2\theta(n_i) = \frac{p+3/2}{p+1/2} \frac{\mathscr{F}_{p+1/2}(\eta_i)}{\mathscr{F}_{p-1/2}(\eta_i)} \frac{\mathscr{F}_{-1/2}(\eta_i)}{\mathscr{F}_{1/2}(\eta_i)} - 1. \tag{45}$$

Shown in the top panel of Fig. 6 are the concentration dependencies of θ for selected values of the scattering exponent p. Since θ is close to unity, the ratio of the Soret current to the usual diffusive current is mainly determined by the relative values of the temperature and charge gradients. While θ is unity for $p = 0$, θ decreases for $p \neq 0$ with increasing concentration from $p+1$ in the nondegenerate limit to unity at very large n_i.

As found from Eq. (30),

$$\frac{K_{++}}{K_{--}} = \frac{\theta(n_+)}{\theta(n_-)} \frac{D_+}{D_-}, \tag{46}$$

so that under degeneracy the Soret current becomes spin-dependent in the same way as diffusion. For $p \neq 0$, $\theta(n_+) < \theta(n_-)$, so that $K_{++}/K_{--} < D_+/D_-$. In this case, the thermal gradient causes an effective decrease of the polarization dip.

C. Hole screening of electron-electron interactions

It is shown here that spin-spin or spin-charge couplings induced by electron-electron interactions are strongly reduced because of screening by the hole gas. The effect of hole screening can be simply taken into account in the random phase approximation (RPA) in the present case where the hole screening is dominant over the electronic one. In this case, the static Coulomb potential in Fourier space is given by [36,37]

$$v(k) = \frac{4\pi e^2}{\epsilon\left(k^2 + k_{DH}^2\right)}, \tag{47}$$

where $e = q/\sqrt{4\pi\epsilon_0}$. The Debye-Hückel screening wave vector k_{DH} depends on the hole concentration according to [38]

$$k_{DH}^2 = \frac{4\pi e^2 N_A}{\epsilon k_B T} \frac{1}{\xi(N_A + \delta p)}, \tag{48}$$

where the function $\xi(x)$ is related to the hole Fermi energy and defined by Eq. (38). In this framework, it seems clear that electron-electron interactions will be decreased if k_{DH} is larger than the typical value of k, of the order of the Fermi wave vector $k_{Fi} = (6\pi^2 n_i)^{1/3}$.

Such reasoning is applied to the calculation of the spin stiffness S_{ii} in the presence of electron-electron exchange interactions (band-gap renormalization). This calculation is detailed in Appendix C to first order and the result is given by Eq. (C5) in the low-temperature limit. Curve a of the top panel of Fig. 7 shows the spin stiffness dependence on the electron concentration n_i at 4 K. Curve b and curve c show the same quantity for unscreened and screened $[N_A + \delta p = 10^{18}\,\mathrm{cm}^{-3}]$ exchange interactions, respectively. In the absence of screening, exchange interactions induce a significant decrease of the spin stiffness, and therefore of

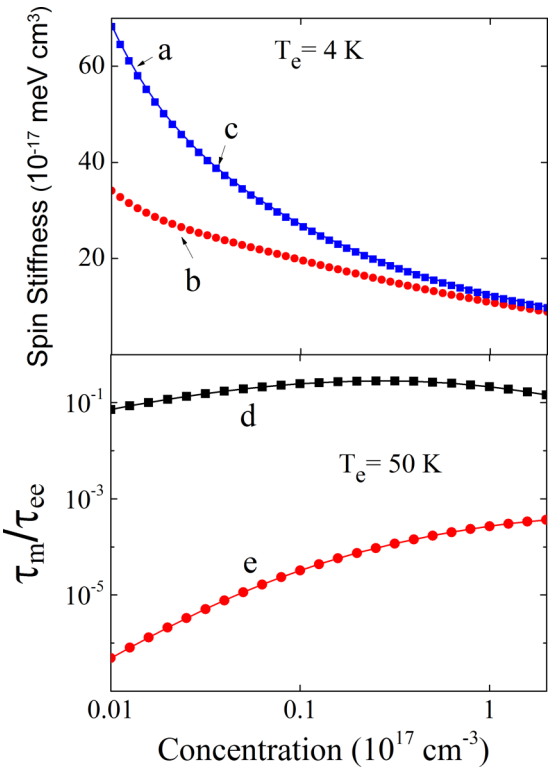

FIG. 7. (Color online) Effect of electron-electron interactions on spin transport in p^+ GaAs. The top panel shows the dependence as a function of n_i of the spin stiffness S_{ii} [see Eq. (22)] without exchange interactions (curve a), while the full circles (curve b) and the full squares (curve c) show the same quantity for unscreened exchange interactions and screened interactions, respectively [see Eq. (C1)]. The bottom panel shows the effect of screening on the efficiency of Coulomb spin drag. Curve d shows the quantity τ_m/τ_{ee}, calculated in Appendix C, as a function of the electron concentration without any screening by holes, and corresponds to results of Ref. [15]. The screening by holes of concentration $N_A^- = 10^{18}\,\mathrm{cm}^3$ is included in curve e. The strong screening-induced decrease of τ_m/τ_{ee} shows that, for the present material, spin drag is negligible.

the diffusion constant, as seen from Eq. (37). This decrease is however completely canceled if screening is included, as seen from the perfect correspondence between curve a and curve c. This screening is found to be extremely efficient, since a small value of $N_A + \delta p = 10^{15}\,\mathrm{cm}^{-3}$ is sufficient to produce a complete screening [39]. Although this result has been obtained in the low-temperature limit, the conclusion remains true at higher temperature since the order of magnitude of renormalization corrections tends to decrease [40]. It is thus concluded that, in the presence of screening, electron-electron interactions are completely negligible.

In the case of Coulomb spin drag, the effect of hole screening on the quantity τ_m/τ_{ee} appearing in Eq. (20) is calculated in Appendix C using the theory developed in Refs. [15,41]. The result is shown in the bottom panel of Fig. 7. Without screening, in agreement with Ref. [15], the maximum value of τ_m/τ_{ee} is small but not completely negligible. Its value is about 0.3 and is reached near $n = 10^{16}\,\mathrm{cm}^{-3}$ which corresponds to the limit of degeneracy. For $N_A^- = 10^{18}\,\mathrm{cm}^{-3}$, it is found that the efficiency of spin drag is decreased by three orders of magnitude. As a result, the effect of Coulomb spin drag is completely negligible.

V. INTERPRETATION

A. Calculation of the polarization profiles

In order to determine the relative importance of the various processes considered in Sec IV, we have solved numerically the system of Eq. (33), Eq. (34), Eq. (35), and Eq. (36), using an approximate method described in Appendix B and taking for the front and back surface recombination velocities the very weak values in our low-temperature conditions $S = S' = 5 \times 10^4$ cm/s [26]. The polarization profiles were then calculated using Eq. (1) and Eq. (2). The parameters used for the resolution were all determined independently so that no fitting procedure was used. Their values are given in Sec. II B apart from those of the electronic temperature T_e and scattering exponent p which are discussed now.

The increase of the local temperature T_e of the photoelectron gas caused by the increase of excitation power was first characterized. Shown in the inset of Fig. 8 are local luminescence spectra at high excitation power, as a function of distance to the excitation spot. The spectra exhibit a change in the shape of the high-temperature tail, thus revealing a local heating of the electron gas near the place of excitation. It is assumed that the heating of holes is negligible [34]. Figure 8 itself shows the spatial dependence of T_e at a lattice temperature of 15 K, for several excitation powers. At low power, the temperature is constant and equal to 40 K. Conversely, at the maximum power, $T_e = 80$ K at the place of excitation and decreases to 50 K over a characteristic distance slightly larger than the radius of the laser excitation spot [42].

The scattering exponent p defined in Eq. (16) was estimated using a combined measurement of Hall and drift photoelectron mobility [23]. One finds $p = 0 \pm 0.5$, which is close to the expected value $p = 1/2$ in the case where the mobility is determined by screened collisions with charged impurities or with majority holes [31,43]. This result implies that, for the present sample, the spin dependence of the mobility is weak.

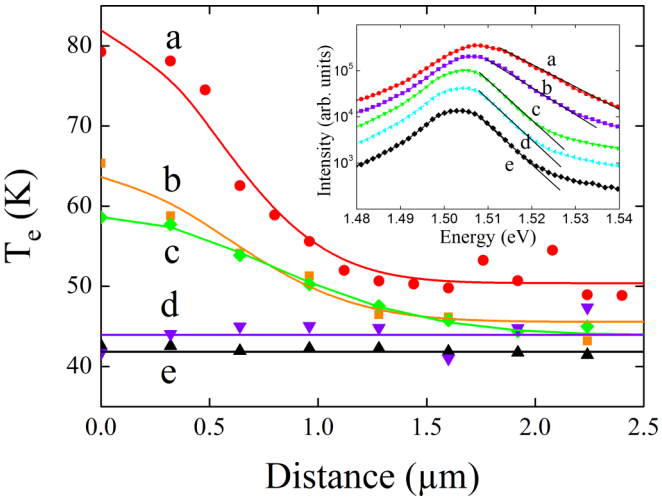

FIG. 8. (Color online) The inset shows, for a large excitation power of 2.5 mW for $T = 15$ K, the spatially resolved luminescence spectra at the place of excitation (a) and at a distance of 0.64 μm (b), 2.7 μm (c), 4 μm (d), and 9.6 μm (e). The larger electronic temperature T_e at the place of excitation is evidenced from the high-energy side of the spectra. The main figure shows T_e as a function of distance for different excitation powers: 2.5 mW (a), 1.9 mW (b), 1 mW (c), 0.45 mW (d), and 1.5 μW (e).

B. Discussion

The calculated polarization profiles are shown in panel (b) of Fig. 2 for the same excitation powers as panel (a). These profiles correspond quite well with the experimental results of panel (a), apart from a slight difference in the position of the polarization maximum. As shown in panel (c) of Fig. 2, the polarization dip is restricted mainly to a zone labeled $\mathscr{D}$, defined by $z < 1$ μm and $r < 0.3$ μm. Conversely, for $r \approx 1.5$ μm and $z < 1$ μm, the polarization maximum is as large as 42%. At the highest excitation power, one calculates that the averages of the concentrations over $\mathscr{D}$ are $\langle n_+(\mathscr{D})\rangle \approx 9.0 \times 10^{16}$ cm^{-3} and $\langle n_-(\mathscr{D})\rangle \approx 5.4 \times 10^{16}$ cm^{-3}. These values are higher than the spin-resolved effective density of states at 80 K which is $N_c^s \approx 3 \times 10^{16}$ cm^{-3}. With these concentrations, we calculate that $D_+ = 1.96 D_0$, $D_- = 1.59 D_0$ so that $D_+/D_- = 1.25$. This value is slightly different from the experimental value of 1.49, which is not surprising because of the approximations used for the latter value.

The importance of ambipolar diffusion is seen from panel (d) of Fig. 2, which shows the profiles calculated in the unipolar case, by considering only Eq. (33) and Eq. (34) and by taking $E = 0$. It is striking to see that, in this case, one observes only a small polarization dip in the profiles at the place of excitation. With the present values of N_A and n, ambipolar diffusion results in reduced ambipolar diffusion constants D_{cc}^a and D_{cs}^a, by the same amount β_h defined by Eq. (B1). The latter quantity can be quite small since at low temperature $\mu_e/\mu_h \approx 85$. This results in an increase of the concentrations and therefore of the amount of degeneracy at $r = 0$. In the unipolar case, we find at the highest excitation power $\langle n_+(\mathscr{D})\rangle \approx 5.2 \times 10^{16}$ cm^{-3} and $\langle n_-(\mathscr{D})\rangle \approx 2.2 \times 10^{16}$ cm^{-3}. The total concentration is smaller than its above ambipolar value by a factor of $\approx$2, in agreement with the qualitative correspondence between the

unipolar calculated profile at 2.5 mW and the experimental one for a reduced power of 1 mW.

Note finally that the concentration in the unipolar case is still larger than N_c^s so that some amount of degeneracy is still present. Indeed we calculate $D_+/D_- = 1.26$, i.e., quite similar to the value at high power. This is because, in Eq. (10), the decrease of δ caused by the smaller concentration is compensated by the polarization increase so that the actual value of D_+/D_- only weakly depends on concentration. On the other hand, the actual value of the polarization in $\mathscr{D}$ is the result of a self-consistent equilibrium and can be relatively sensitive to the concentration [44].

Panel (e) shows the profile calculated under the same conditions as panel (b), except that the Soret charge and spin currents are neglected. Here T_e is taken as spatially homogeneous and equal to its measured value at $r = 0$. Apart from the highest power where the profile is slightly shifted upwards, the profiles are nearly the same as in panel (b), implying that the Soret current plays a negligible role in these experiments [45]. The relative temperature gradient $\vec{\nabla}_r T_e/T_e$ strongly varies with distance. As found from curve a of Fig. 8, its value at high power is very small near $r = 0$, reaches 1.3 μm^{-1} in a very short interval near 0.6 μm, and then decreases to 0.3 μm^{-1}. In comparison, the relative charge gradient $\vec{\nabla}_r n_e/n_e$, found using Fig. 1, is almost independent of distance and is of the order of 1 μm^{-1} and is, within experimental uncertainties, larger than the temperature relative gradient at most distances. Using Eq. (43), it is thus concluded that the temperature gradient is not sufficient to obtain significant Soret currents.

Panel (f) of Fig. 2 shows the polarization profile calculated by considering the unipolar limit without temperature gradients, T_e being fixed to its measured value at $r = 0$. This situation is reminiscent of spatially homogeneous configuration of spin-grating experiments. In this case the polarization dip near $r = 0$ has almost disappeared. Observation of the Pauli blockade driven spin filter effect thus requires spatially inhomogeneous electron and hole concentrations. This means that the usual spin-grating technique, in which the electron and hole concentrations are uniform in space, may not be well adapted to the observation of Pauli blockade effects in spin transport. On the other hand, for spin gratings, T_e is also uniform in space, meaning that the charge and spin Soret effects are absent, a situation which should slightly increase the magnitude of Pauli blockade phenomena. Given that heating of the photoelectron gas is unavoidable during high-intensity photoexcitation, the ideal conditions for measuring the largest possible Pauli blockade effects are highly inhomogeneous photoelectron and hole concentrations and spatially uniform temperatures.

VI. CONCLUSION

Here, we present a theoretical and experimental investigation of the effect of degeneracy on spin transport of a photoelectron gas. We have used p^+ GaAs for which at 15 K tightly focused circularly polarized light excitation generates strongly spin-polarized photoelectrons (45%) and where charge and polarization profiles are monitored as a function of distance. We now recall the main results.

(a) In conditions where the photoelectron gas is degenerate, i.e., for a sufficiently low temperature and large excitation power (above 1 mW), we demonstrate a spin-charge coupling mechanism implying a spin dependence of the diffusive transport, with relative differences in the spin-resolved diffusion constants as large as 50% between the two types of spins. This effect is linear in the electronic polarization, increases with the electron concentration, and decreases with increasing kinetic energy in the conduction band. The spin-averaged charge diffusion constant is also shown to be spin-dependent due to a second-order effect. The dominant effect which explains these results is the charge and spin dependence of the spin stiffness under degeneracy.

(b) Ambipolar diffusion plays a key role for the observation of spin-dependent diffusion, since it increases the confinement of photoelectrons at the place of excitation, and therefore the amount of degeneracy, due to the electrostatic electron-hole coupling. This diffusion induces a strongly nonlinear coupling between electron diffusion, spin diffusion, and hole diffusion, which is treated here using an approximate resolution of the diffusion equations. Such ambipolar-induced increase of the confinement could also be obtained by increasing the excitation power, but this will inevitably increase the electron temperature and decrease the degeneracy.

(c) The mobility is predicted to depend on charge and on spin. However, for p^+ GaAs, this effect is weak. This conclusion is at variance with the hypothesis of the previous work [14] and is based on recent measurements of the dependence of the scattering time on kinetic energy [23], as defined by the value of p in Eq. (16). The value of p is found to be strongly reduced from $3/2$ due to scattering with charged impurities, as a consequence of the screening by holes. It is anticipated that the spin dependence of the mobility should be observable at a lower p-type doping.

(d) Since the electronic temperature is strongly inhomogeneous, thermoelectric currents may appear due to the Soret effect, which are predicted to depend on spin in degenerate conditions. However, in the present situation, this dependence does not strongly affect the polarization profile because of the relative values of charge and temperature gradients. Distinct experimental configurations should be used for separate investigation of this effect.

(e) Other spin-spin or spin-charge coupling mechanisms such as spin drag or band-gap renormalization are negligible in the present case because of efficient screening of the electron-electron interactions by the holes of our p^+ material.

In summary, the extensive theoretical analysis of the present work and the careful sample characterization allow us to conclude that we have achieved experimentally a relatively simple situation, where the polarization profiles mostly depend on spin-dependent ambipolar diffusion under degeneracy. It is predicted that other effects could play a role under degeneracy such as spin-dependent mobility or Soret currents. These effects remain unobserved and could be explored by adjusting the acceptor density and the laser energy and power. Note that the present technique relying on a tightly focused laser excitation seems better adapted than the elegant spin-grating technique for investigating the effect of degeneracy on spin transport. The main reason is that effects of degeneracy on pure spin currents created in the latter technique are not amplified by ambipolar diffusion. They decrease under increase of

excitation power because of the unavoidable heating of the electron gas which reduces the degree of degeneracy.

It is finally pointed out that these large spin-dependent effects have been observed in a regime near the onset of degeneracy, where the photoelectron concentrations are not very large with respect to the effective density of states in the conduction band. This implies that much stronger effects are expected for larger powers. While this is not possible in the present case because of heating effects, we anticipate that the use of appropriate low-dimensional structures of reduced effective density of states will increase the magnitude of the effects and may possibly open the way to the realization of spin components of increased diffusion length and mobility at a temperature closer to 300 K.

ACKNOWLEDGMENTS

We are grateful to J.-P. Korb and D. Grebenkov for valuable help in the characterization of the sample dynamic properties. We thank E. L. Ivchenko and S. A. Tarasenko for extremely fruitful discussions. One of us (F.C.) is grateful to Becas de doctorado en el extranjero, Becas Chile for supporting his work.

APPENDIX A: BOLTZMANN EQUATION FORMALISM FOR THE CHARGE, SPIN, AND THERMOELECTRIC CURRENTS

The current $\vec{J}_i$ of photoelectrons of spin i is given by

$$\vec{J}_i = -\frac{q}{m^*}\int \vec{p}\, f_i d^3p, \tag{A1}$$

where the function f_i, which describes the distribution of electrons of spin i as a function of space and of momentum $\vec{p}$, is obtained from a resolution of the Boltzmann equation

$$\frac{\partial f_i}{\partial t} + \vec{p}\vec{\nabla}_r f_i - \frac{q\vec{E}}{m^*}\nabla_k f_i = \left[\frac{\partial f_i}{\partial t}\right]_{icoll} + \left[\frac{\partial f_i}{\partial t}\right]_{e-ecoll}, \tag{A2}$$

where the second term on the left-hand side accounts for the effect of diffusion in a Fermi energy gradient. The third term describes the effect of electric field and the two terms on the right-hand side are collision integrals accounting for electron-impurity collisions and electron-electron collisions.

The models of Refs. [15,46,47] propose estimates of the collision integrals, but do not take into account spatial inhomogeneities of f. These inhomogeneities are considered in an independent approach, which however neglects the spin polarization, so that electron-electron collisions have no effect [48]. Here, neglecting band nonparabolicity, we propose the following ansatz to first order which reduces to the result of Ref. [15] for a homogeneous electron gas and to that of Ref. [48] for spin-unpolarized electrons:

$$f_i = f_{0i} - \frac{\alpha_{ii}\tau_m(\varepsilon)}{m^*}[-q\vec{E}\cdot\vec{\nabla}_\varepsilon f_{0i} + \vec{p}\cdot\vec{\nabla}_r f_{0i}] - \frac{\alpha_{i,-i}\tau_m(\varepsilon)}{m^*}[-q\vec{E}\cdot\vec{\nabla}_\varepsilon f_{0,-i} + \vec{p}\cdot\vec{\nabla}_r f_{0,-i}], \tag{A3}$$

where for noncoupled spins ($\alpha_{i,-i} = 0$) one recognizes the usual drift term in the electric field $\vec{E}$ and the diffusion term proportional to the spatial gradient $\vec{\nabla}_r f_{0i}$ [48]. In order to take account of the spin-spin interactions for the evolution of f_i, it is natural to add a coupling term with the evolution of f_{-i}, using the same coupling factor $\alpha_{i,-i}$ as the one given by Eq. (20), which describes the modification of conductivity $\sigma_{i,-i}$ caused by e-e collisions. In the same way, the evolution of f_i is also modified by losses to the $-i$ spin system, which are taken into account by the multiplicative factor α_{ii}. It is considered here that $\tau_m(\varepsilon)$ does not depend on spin, since the spin dependence of τ_{mi} used in Sec. II originates from the sole spin dependence of the Fermi distribution. Equation (A1) allows us to calculate the currents using Eq. (A3) and

$$\vec{\nabla}_r f_{0i} = -\frac{\partial f_{0i}}{\partial\varepsilon}\cdot\left[\sum_j \frac{\partial E_{F_i}}{\partial n_j}\vec{\nabla}_r n_j + \left(\frac{\partial E_{F_i}}{\partial k_B T_e} + \frac{E - E_{F_i}}{k_B T_e}\right)\vec{\nabla}_r(k_B T_e)\right]. \tag{A4}$$

Since the contribution of the equilibrium term f_0 is zero, the current is written as the sum of a drift current, of a diffusion current, and of a thermoelectric current, respectively proportional to $\vec{E}$, $\vec{\nabla}_r n$, and $\vec{\nabla}_r(k_B T)$. This gives the expressions of the drift and diffusion currents given in Sec. III A 1. Transforming the integration over momentum to an integration over kinetic energy, the expression of the average time τ_{mi} given by Eq. (15) is readily obtained. The thermoelectric charge and spin currents originate from the second term of Eq. (A4). The thermal-induced change of E_{F_i} at constant concentration, $\partial E_{F_i}/\partial k_B T_e$, is calculated by expressing that the derivative of n_i with respect to temperature, as found from Eq. (6), is zero. Using $\partial\mathscr{F}_k^*(\eta)/\partial\eta = \mathscr{F}_{k-1}^*(\eta)$, one finds the expression given in Eq. (30) for $\vec{K}_{ij}$.

APPENDIX B: SOLUTION OF THE EQUATIONS FOR AMBIPOLAR SPIN DIFFUSION

In contrast with the usual treatments of ambipolar diffusion [31,49], the system of Eq. (33), Eq. (34), Eq. (35), and Eq. (36) must be solved numerically since the conductivities and diffusion constants depend on space. However, an exact numerical solution of these equations is difficult, since small errors in n and δp result in large errors in $\vec{E}$. This renders the equations highly nonlinear and a convergent solution is difficult to obtain using finite-element methods without approximations. To address this, the hole continuity equation is replaced by a combination of Eqs. (33) (multiplied by σ_h) and (35) (multiplied by σ_c) in the usual way [31]. Defining the reduced hole conductivity $\beta_h = \sigma_h/(\sigma_h + \sigma_c)$, of the form

$$\beta_h = \frac{N_A^- + n}{(N_A^- + n) + (\mu_0/\mu_h)[n_+\zeta(n_+) + n_-\zeta(n_-)]}, \tag{B1}$$

the following equation to describe the hole distribution is obtained:

$$(g_+ + g_-) - \delta p/\tau + \frac{\vec{E}}{q}\vec{\nabla}\sigma_c^a + \vec{\nabla}\left[D_{cc}^a\vec{\nabla}\delta p + D_{cs}^a\vec{\nabla}s + \frac{1}{q}\beta_h\vec{\nabla}\vec{J}_c^T\right] = 0, \quad \text{(B2)}$$

where

$$D_{cc}^a = \beta_h D_{cc} + (1-\beta_h)D_h, \quad \text{(B3)}$$

$$D_{cs}^a = \beta_h D_{cs}, \quad \text{(B4)}$$

and $\vec{\nabla}\sigma_c^a = \beta_h\vec{\nabla}\sigma_c - (1-\beta_h)\vec{\nabla}\sigma_h$. Equation (B2) is approximate since, as justified in Ref. [18], it assumes charge neutrality [$n = \delta p$]. Further, it neglects for simplicity the spatial dependencies of electron and hole conductivities. However, this approximation appears to yield reasonable results. For example, at the highest excitation power where the equations are most strongly coupled, the sum of all the terms on the left-hand side of Eq. (33) is two orders of magnitude smaller than the maximum value of $\vec{\nabla}\cdot[D_{cc}\vec{\nabla}n]$ so that these terms efficiently compensate each other.

APPENDIX C: EFFECT OF SCREENING BY HOLES ON ELECTRON-ELECTRON INTERACTIONS

(a) We first estimate the contribution of electron-electron interactions to the electron spin stiffness in the presence of a degenerate hole gas. The electron mutual interactions in the electron gas lead to a self-energy correction to the bare electron energy, usually split into exchange and correlation terms and given by $\Sigma_{i,k} = \Sigma_{i,k}^x + \Sigma_{i,k}^{cor}$. The effective Fermi energy is then given by $E_{Fi}^* = E_{Fi} + \langle\Sigma_{i,k}^x\rangle$ where $\langle\ \rangle$ denotes the average over all electrons of spin i and the contribution of many-body effects to the spin stiffness is thus given by

$$S_{i,j}^{xc} = \frac{\partial\langle\Sigma_{i,k}^x\rangle}{\partial n_j}\delta_{i,j} + \frac{\partial\langle\Sigma_{i,k}^{cor}\rangle}{\partial n_j}, \quad \text{(C1)}$$

since the exchange correction is computed within a population of electrons of the same spin i. In degenerate conditions, we will neglect the contribution of the correlation energy, which is small with respect to the exchange one [40] and the spin stiffness matrix is diagonal. At low temperature, one has $\Sigma_{i,k}^x = -(1/V)\sum_q v(q) f_{i,k+q}$ where V is the sample volume and $v(q)$ is the screened potential given by Eq. (47). The exchange energy for electrons of momentum k and spin i can be analytically computed as

$$\Sigma_{i,k}^x = -\frac{e^2 k_{Fi}}{\epsilon\pi}\mathscr{B}\left(\frac{k}{k_{Fi}}, \frac{k_{DH}}{k_{Fi}}\right), \quad \text{(C2)}$$

where the negative function $\mathscr{B}$ is given by

$$-\mathscr{B}(y_1,y_2) = 1 + y_2\arctan\frac{y_1-1}{y_2} + y_2\arctan\frac{y_1+1}{y_2} + \frac{1+y_2^2-y_1^2}{4y_1}\ln\frac{(1+y_1)^2+y_2^2}{(1-y_1)^2+y_2^2} \quad \text{(C3)}$$

and reduces to the usual expression [36,50] in the absence of holes. After integration over all electrons of spin i, the average exchange energy is written

$$\langle\Sigma_{i,k}^x\rangle = \frac{3e^2 k_{Fi}}{2\epsilon\pi}\int_0^1 y_1^2\mathscr{B}\left(y_1, \frac{k_{DH}}{k_{Fi}}\right)dy_1 \quad \text{(C4)}$$

and the additional spin stiffness is given by

$$S_{i,i}^x = \left[\frac{3}{4\pi}\right]\frac{e^2}{\epsilon}\int_0^1 y_1^2\mathscr{R}\left(y_1, \frac{k_{DH}}{k_{Fi}}\right)n_i^{-2/3}dy_1, \quad \text{(C5)}$$

where

$$-\mathscr{R}(y_1,y_2) = 1 + \frac{1+y_2^2-y_1^2}{4y_1}\ln\frac{(1+y_1)^2+y_2^2}{(1-y_1)^2+y_2^2}. \quad \text{(C6)}$$

(b) We now estimate the effect of screening on spin drag. The relative efficiency of spin drag under screening is measured from the ratio $\tau_m/\tau_{ee} = \rho_{+-}\sigma_c$ where the spin transresistivity ρ_{+-} is expressed as an integration over frequency followed by an integration over momentum [15,41]:

$$\rho_{+-} = \frac{\hbar^2}{q^2 n_+ n_-}\frac{1}{3\pi^3}\int_0^\infty k^4 v(k)^2 dk \times \int_0^\infty d\omega \frac{\chi_{0+}''(k,\omega)\chi_{0-}''(k,-\omega)}{|\epsilon(k,\omega)|^2\sinh^2(\hbar\omega/2k_BT)}, \quad \text{(C7)}$$

where the dynamic dielectric constant is given by

$$\epsilon(k,\omega) = 1 - v(k)[\chi_{0+}(k,\omega) + \chi_{0-}(k,\omega)]. \quad \text{(C8)}$$

Here, $\chi_{0i}(k,\omega)$ is the noninteracting spin-resolved density-density response function of spins i and $\chi_{0i}''(k,\omega)$ is its imaginary part. The expressions of the latter quantities can be found in Ref. [41]. Since $\chi_{0i}''(k,\omega)$ does not directly depend on the potential, it is natural to include the effect of screening by holes by using for the potential $v(k)$, the expression given by Eq. (47).

[1] J. Wunderlich, Science **330**, 1801 (2010).
[2] T. Jungwirth, J. Wunderlich, and K. Olejnik, Nat. Mater. **11**, 382 (2012).
[3] C. P. Weber, N. Gedik, J. E. Moore, J. Orenstein, J. Stephens, and D. D. Awschalom, Nature (London) **437**, 1330 (2005).
[4] J. D. Koralek, C. P. Weber, J. Orenstein, B. A. Bernevig, S. C. Zhang, S. Mack, and D. D. Awschalom, Nature (London) **458**, 610 (2009).
[5] S. Datta and B. Das, Appl. Phys. Lett. **56**, 665 (1990).
[6] I. Zutic, J. Fabian, and S. C. Erwin, J. Phys.: Condens. Matter **19**, 165219 (2007).
[7] N. C. Gerhardt, M. Y. Li, H. Jahme, H. Hopfner, T. Ackemann, and M. R. Hofmann, Appl. Phys. Lett. **99**, 151107 (2011).
[8] A. R. Cameron, P. Riblet, and A. Miller, Phys. Rev. Lett. **76**, 4793 (1996).
[9] V. S. Zapasskii, A. Greilich, S. A. Crooker, Yan Li, G. G. Kozlov, D. R. Yakovlev, D. Reuter, A. D. Wieck, and M. Bayer, Phys. Rev. Lett. **110**, 176601 (2013).

[10] G. Wang, A. Balocchi, D. Lagarde, C. R. Zhu, T. Amand, P. Renucci, Z. W. Shi, W. X. Wang, B. L. Liu, and X. Marie, Appl. Phys. Lett. **102**, 242408 (2013).

[11] G. Wang, B. L. Liu, A. Balocchi, P. Renucci, C. R. Zhu, T. Amand, C. Fontaine, and X. Marie, Nat. Commun. **4**, 2372 (2013).

[12] A. Balocchi, Q. H. Duong, P. Renucci, B. L. Liu, C. Fontaine, T. Amand, D. Lagarde, and X. Marie, Phys. Rev. Lett. **107**, 136604 (2011).

[13] Y. Takahashi, N. Inaba, and F. Hiroshe, J. Appl. Phys. **104**, 023714 (2008).

[14] F. Cadiz, D. Paget, and A. C. H. Rowe, Phys. Rev. Lett. **111**, 246601 (2013).

[15] I. D'Amico and G. Vignale, Phys. Rev. B **65**, 085109 (2002).

[16] Y. Qi, Z. G. Yu, and M. E. Flatte, Phys. Rev. Lett. **96**, 026602 (2006).

[17] I. Favorskiy, D. Vu, E. Peytavit, S. Arscott, D. Paget, and A. C. H. Rowe, Rev. Sci. Instrum. **81**, 103902 (2010).

[18] D. Paget, F. Cadiz, A. C. H. Rowe, F. Moreau, S. Arscott, and E. Peytavit, J. Appl. Phys. **111**, 123720 (2012).

[19] F. Cadiz, D. Paget, A. C. H. Rowe, V. L. Berkovits, V. P. Ulin, S. Arscott, and E. Peytavit, J. Appl. Phys. **114**, 103711 (2013).

[20] S. D. Brechet and J. P. Ansermet, arxiv:1011.2323v1.

[21] J. S. Blakemore, J. Appl. Phys. **53**, R123 (1982).

[22] F. Meier and B. Zakharchenya, *Optical Orientation* (North-Holland, Amsterdam, 1984).

[23] F. Cadiz, D. Paget, A. C. H. Rowe, E. Peytavit, and S. Arscott, Appl. Phys. Lett. **106**, 092108 (2015).

[24] S. I. Kim, C. S. Son, S. W. Chung, Y. K. Park, E. K. Kim, and S. K. Kim, Thin Solid Films **310**, 63 (1997).

[25] D. R. Luber, F. M. Bradley, N. M. Haegel, M. C. Talmadge, M. P. Coleman, and T. D. Boone, Appl. Phys. Lett. **88**, 163509 (2006).

[26] F. Cadiz, P. Baratte, D. Paget, D. Grebenkov, J. P. Korb, A. C. H. Rowe, T. Amand, S. Arscott, and E. Peytavit, J. Appl. Phys. **116**, 023711 (2014).

[27] K. Zerrouati, F. Fabre, G. Bacquet, J. Bandet, J. Frandon, G. Lampel, and D. Paget, Phys. Rev. B **37**, 1334 (1988).

[28] M. S. Feng, C. S. A. Fang, and H. D. Cheng, Mater. Chem. Phys. **42**, 143 (1995).

[29] H. C. Casey and F. Stern, J. Appl. Phys. **47**, 631 (1976).

[30] R. Volkl, M. Griesbeck, S. A. Tarasenko, D. Schuh, W. Wegscheider, C. Schuller, and T. Korn, Phys. Rev. B **83**, 241306(R) (2011).

[31] R. A. Smith, *Semiconductors* (Cambridge University Press, Cambridge, 1978).

[32] M. Cutler and N. F. Mott, Phys. Rev. **181**, 1336 (1969).

[33] C. Soret, Archives des Sciences Physiques et Naturelles, Geneve **2**, 48 (1879).

[34] K. Leo and J. H. Collet, Phys. Rev. B **44**, 5535 (1991).

[35] A. M. Finkel'shtein, Sov. Phys. JETP **57**, 97 (1983).

[36] G. D. Mahan, *Many-Particle Physics* (Plenum, New York, London, 1981).

[37] J. H. Collet, Phys. Rev. B **47**, 10279 (1993).

[38] J. Collet and T. Amand, J. Phys. Chem. Solids **47**, 153 (1986).

[39] This result should only be taken qualitatively, since in this case, the electron concentration is larger than the hole one so that screening by electrons should also be taken into account in a calculation to second order.

[40] We have checked, using Refs. [50,51], that for $T_e = 60$ K and $n = 10^{16}$ cm^3, the exchange term dominates the electron gas energy, and can be approximated by its value at $T_e = 0$ K.

[41] G. F. Giuliani and G. Vignale, *Quantum Theory of the Electron Liquid* (Cambridge University Press, Cambridge, UK, 2005).

[42] The heating of the electron gas is given by the approximate balance equation $C_v(T_e - T)/\tau_{\rm eff}(0) = g(0)\Delta E/n(0) - [dE/dt]_{\rm phon}$. Here $C_v \approx 3k_B T_e/2$ is the heat capacitance per electron, ΔE is the energy per electron given to acoustic modes, and $[dE/dt]_{\rm phon}$ is the rate of energy exchange to the phonons, calculated in Ref. [52]. Using this simple equation, we find $\Delta E = 15$ meV, in good agreement with the initial kinetic energy after emission of two optical phonons.

[43] D. Chattopadhyay and H. J. Queisser, Rev. Mod. Phys. **53**, 745 (1981).

[44] Another effect of ambipolar diffusion is to introduce an electrostatic coupling between spins + and spins − via the holes so that the ambipolar diffusion matrix D^a_{ij} is not diagonal. This can be seen in the simpler case where the concentrations are spatially homogeneous, by performing linear combinations of the hole diffusion equation and of the diffusion equations for spins ± respectively, in the same way as in Ref. [31].

[45] Since the spin dependence of the Soret current is the same as that of the diffusive current [see Eq. (46) for $\theta = 1$], inclusion of the Soret current essentially does not modify p. On the other hand, at the highest power, there occurs a slight decrease of the concentration by the Soret current, which increases the polarization.

[46] K. Flensberg, T. S. Jensen, and N. A. Mortensen, Phys. Rev. B **64**, 245308 (2001).

[47] M. M. Glazov and E. I. Ivchenko, JETP **99**, 1279 (2004).

[48] A. N. Chakravarti, Czech. J. Phys. B **25**, 778 (1975).

[49] H. Zhao, M. Mower, and G. Vignale, Phys. Rev. B **79**, 115321 (2009).

[50] J. Sun, J. P. Perdew, and M. Seidl, Phys. Rev. B **81**, 085123 (2010).

[51] E. W. Brown, J. L. DuBois, M. Holzmann, and D. M. Ceperley, Phys. Rev. B **88**, 081102(R) (2013).

[52] M. Pugnet, J. Collet, and A. Cornet, Solid State Commun. **38**, 531 (1981).